

Chaotic dynamics in a macrospin spin-torque nano-oscillator with time-delayed feedback

Jérôme Williams,^{1, a)} Artur Difini Accioly,¹ and Joo-Von Kim^{1, b)}

Centre de Nanosciences et de Nanotechnologies, CNRS, Univ. Paris-Sud, Université Paris-Saclay, 91405 Orsay, France

(Dated: 14 September 2017)

A theoretical study of delayed feedback in spin-torque nano-oscillators is presented. A macrospin geometry is considered, where self-sustained oscillations are made possible by spin transfer torques associated with spin currents flowing perpendicular to the film plane. By tuning the delay and amplification of the self-injected signal, we identify dynamical regimes in this system such as chaos, switching between precession modes with complex transients, and oscillator death. Such delayed feedback schemes open up a new field of exploration for such oscillators, where the complex transient states might find important applications in information processing.

Spin-torque nano-oscillators (STNO) are nanoscale electrical oscillators based on ferromagnetic materials that are promising for a number of technological applications, such as microwave sources and field sensors.¹⁻³ They are typically based on magnetoresistive stacks, whereby spin-torques exerted by the flow of spin-polarized currents result in the self-sustained oscillation of the magnetization in the free layer.⁴⁻⁷ The oscillation state can comprise (quasi-)uniform precession,^{8,9} spin wave bullets,¹⁰ gyrating vortices¹¹⁻¹⁵ and skyrmions,¹⁶ and dynamical droplet solitons.¹⁷

Delayed feedback in dynamical systems, whereby the output signal of a system is sent back into its input with amplification and delay, can result in a variety of nonlinear behaviors.¹⁸ One important consequence of delayed feedback is the possibility of inducing chaotic dynamics, even in low-dimensional systems. From a mathematical perspective, the delayed feedback expands the phase space of the dynamical system, which means that phenomena such as chaos can appear. A well-known example is the Mackey-Glass oscillator,¹⁹ which is described by a first-order delay-differential equation and can exhibit a variety of different dynamical states, including limit-cycle and aperiodic states, and complex transients. Indeed, such a dynamical system has recently been implemented in an optoelectronic circuit to perform reservoir computing.²⁰

For the STNO, whose dynamics is well-described by a two-dimensional dynamical system⁷, it is intriguing to inquire whether delayed feedback lead to more complex behavior such as chaos, much like periodic forcing.²¹ It has been shown that delayed feedback can improve spectral properties such as the emission linewidth.²²⁻²⁴ Here, we will present results of a theoretical study on the complex transient response and chaotic behavior in STNOs subject to delayed feedback. We considered a model oscillator system in which the output is generated by changes in the magneto-resistance, which is subsequently fed back as variations in the input drive current. An interesting example is the macrospin²⁵ oscillator operating near the transition between the in-plane (IPP) and out-of-plane (OPP) precession regimes. By tuning the delay and amplification of the self-injected signal, we identify dynamical regimes

in this system such as chaos, IPP/OPP switching with complex transients, and oscillator death.

The macrospin dynamics is described by the Landau-Lifshitz equation with spin torques,²⁶

$$\frac{d\mathbf{m}}{dt} = -\frac{\gamma_0}{1 + \alpha^2} \mathbf{m} \times \mathbf{H}_{\text{eff}} + \gamma_0 \mathbf{m} \times [\mathbf{m} \times (-\alpha \mathbf{H}_{\text{eff}} + J\mathbf{p})], \quad (1)$$

where $\gamma_0 = \mu_0\gamma$ is the gyromagnetic constant, \mathbf{m} is a unit vector representing the magnetization state, \mathbf{H}_{eff} is the effective field, α is the Gilbert damping constant, J is the applied current density, and \mathbf{p} is orientation of the spin polarization. Note that J is expressed as a magnetic field, where a density of 10^7 A/cm² corresponds to a field of 10 mT, which is consistent with spin valve nanopillar devices based on Co/Cu/Co.⁸ In our calculations, we assume a thin film geometry in which z is the direction perpendicular to the film plane with a uniaxial anisotropy and an applied field along the x axis. As such, $\mathbf{H}_{\text{eff}} = (H_0 + H_{\text{an}}m_x)\hat{\mathbf{x}} - H_d m_z \hat{\mathbf{z}}$. In what follows, we used $\mu_0 H_0 = 0.1$ T, $\mu_0 H_{\text{an}} = 0.05$ T, and $\mu_0 H_d = 1.7$ T, which are similar to values considered elsewhere.^{8,27} We take $\mathbf{p} = \hat{\mathbf{x}}$ which defines the parallel configuration.

Some possible precession modes are illustrated in Fig. 1. As established previously,²⁵ the onset of self-sustained oscillations first involves precession of the magnetization in the film plane (IPP), where the trajectory takes the shape of a clamshell centered about the x axis. As the current is increased, the preferred oscillation mode involves out-of-plane precession (OPP), where the axis of precession is the film normal and the orbits are more circular. Note that for this mode there are two degenerate states, i.e., precession about the $+z$ and $-z$ axes, which we denote as (OPP+) and (OPP-), respectively.

The current dependence of the mean values of the three magnetization components and the oscillation period (of the m_x component) is presented in Fig. 2. We observe a clear current threshold at $J \approx 0.007$ T, below which the magnetization remains static along x . Above this threshold in the IPP regime, the average $\langle m_x \rangle$ component (linked to magnetoresistance variations) decreases rapidly as a function of current density, which is also accompanied by a sharp decrease in the oscillation frequency. Note that the average values are $\langle m_y \rangle = \langle m_z \rangle = 0$ in this regime. Above a second threshold, $J \approx 0.015$ T, the system enters the OPP state where all magne-

^{a)}Electronic mail: jerome.williams@c2n.upsaclay.fr

^{b)}Electronic mail: joo-von.kim@c2n.upsaclay.fr

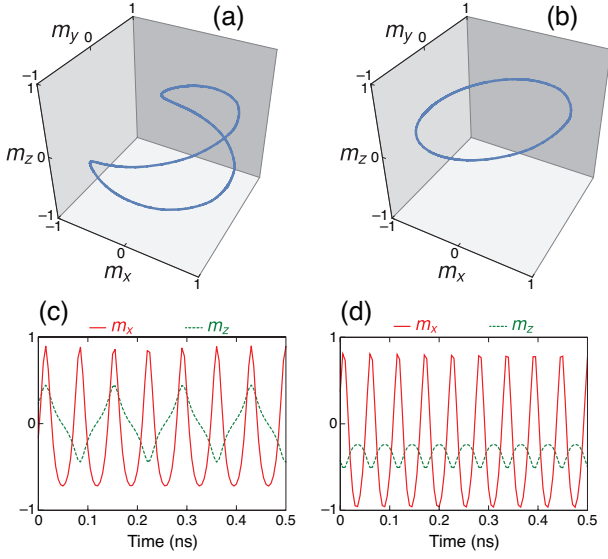


FIG. 1. Oscillation modes of a macrospin spin-torque nano-oscillator. Trajectories and time traces of in-plane precession (IPP) and out-of-plane precession (OPP) precession: (a) IPP trajectory, (b) OPP trajectory, (c) IPP time trace, (d) OPP time trace. Applied currents are $J = 0.01$ T for IPP and $J = 0.02$ T for OPP.

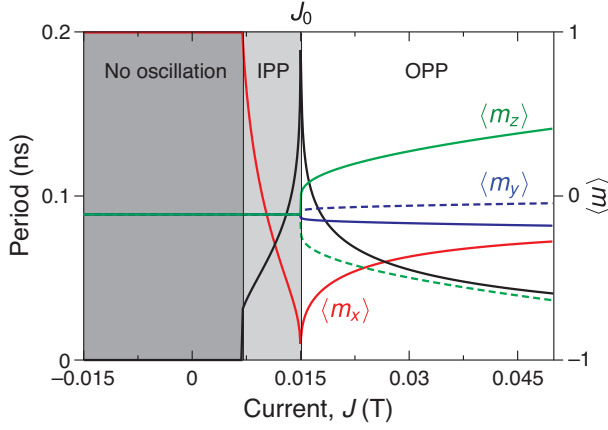


FIG. 2. Mean values of the magnetization components and oscillation period as a function of applied current J . The mean values of m_y and m_z are non-zero only in the OPP mode, while m_x for the non-oscillating mode remains constant at 1. We can identify three dynamical regimes (no oscillation, IPP, and OPP) based on these time-averaged values. J_0 denotes the constant drive current used in this study.

tization components have nonzero time averages. The current dependence of $\langle m_x \rangle$ exhibits the opposite behavior compared with the IPP state, where it progressively increases and is accompanied by an increase in the oscillation frequency. The dashed lines in Fig. 2 indicate the degenerate OPP state. As we will discuss in more detail in the following, these average magnetization components will allow us to identify the different precession states under delayed feedback.

The output signal of a spin-torque nano-oscillator is typically determined by the giant or tunnel magneto-resistance

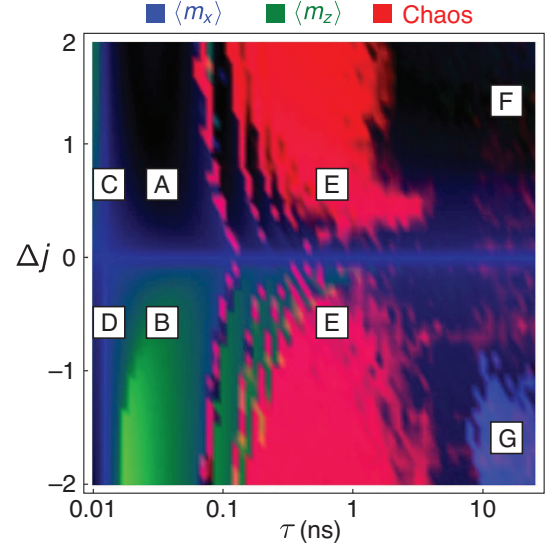


FIG. 3. Phase diagram of possible dynamics as a function of the feedback amplitude Δj and time delay τ . This color-map is constructed using a red-green-blue scheme where the red component is a measure of the chaos, the green represents the time-averaged out-of-plane component m_z , and the blue represents the time-averaged value of m_x . The possible states are (A, D) IPP, (B, C) OPP, (E) chaotic dynamics, (F) unstable precessions, and (G) oscillator death.

effect, where the electrical resistance depends on the relative orientation between the free and reference layer magnetizations. As such, it is natural to employ the output current (or voltage) variation as the feedback signal. We can therefore assume a time-dependent applied current density of the form

$$J(t) = J_0 [1 + \Delta j m_x(t - \tau)], \quad (2)$$

where J_0 is the injected dc current, Δj is the relative feedback amplitude, and τ is a variable time delay. We note that only the m_x component enters since we have assumed that the reference magnetization is oriented along x .

We are interested in the effect of time-delay feedback when the oscillator is operating close to the IPP to OPP transition. To this end, we consider a constant drive current of $J_0 = 0.015$ T, which leads to IPP dynamics but is close to the threshold current for the OPP region. In Fig. 3, we present the full phase diagram of the oscillator behavior as a function of the time delay τ and feedback amplitude Δj . We considered time delays over several orders of magnitude, which allows us to probe different time scales from single precession periods over to longer transients. The phase diagram is represented using a composite red-green-blue color scheme, where the blue component is a measure of the time-averaged in-plane component of the magnetization, $\langle m_x \rangle$, the green component represents $\langle m_z \rangle$, and the red component indicates the existence of chaos. A number of different qualitative behaviors are observed, which are denoted by the capital letters ‘A’ to ‘G’.

Regions ‘A’ and ‘B’ represent the usual IPP and OPP states, respectively, where the sign of the feedback amplitude favors one over the other. This can be understood by examining the

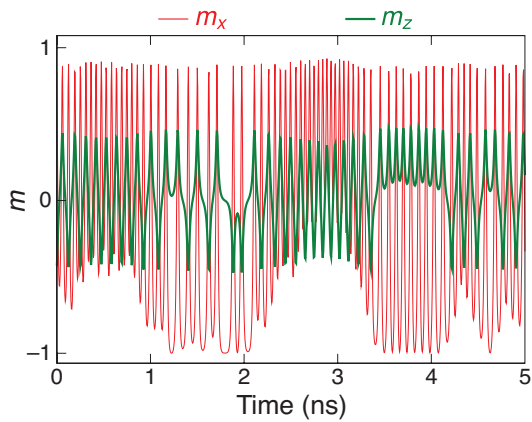


FIG. 4. Representative time trace of chaotic dynamics in region ‘E’ of Fig. 3. The magnetization switches chaotically between IPP and OPP modes as shown by the time evolution of the m_z component.

sign of $\langle m_x \rangle$, which when combined with the feedback determines whether the average applied current leads to the IPP or OPP dynamics, as shown in Fig. 2; $\langle m_x \rangle < 0$ around the IPP/OPP transition, so a negative feedback ($\Delta j < 0$) will drive the system into the OPP regime, while a positive feedback ($\Delta j > 0$) will drive the system further into the IPP regime, away from the IPP/OPP threshold.

For very small time delays (regions ‘C’ and ‘D’), which represent a fraction of the typical precession periods ~ 0.1 ns, we see a reversal of the IPP and OPP position on the feedback amplitude axis. Although this is clearly different from what takes place in regions A and B, the STNO trajectories are very close to the usual IPP/OPP orbits and are practically indistinguishable from them. However, their inverted positions along the Δj axis with respect to the ‘C’ and ‘D’ regions indicate a different physical process at play. We will return to this point later after the following discussion.

When the time delay becomes comparable to the precession period, we begin to see signatures of chaotic dynamics that appear as a result of the feedback. Because of the complex oscillatory nature of STNOs, and the added layer of complexity arising from the feedback loop, a calculation of the maximal Lyapunov exponent²⁸ to characterize chaos is numerically demanding. Instead, we employ a simpler method that allows us to obtain a qualitative measure of chaos. After the delayed feedback is switched on in the simulation, we let the system evolve so that the initial transients have died out. We then designate this state (t_0, \mathbf{m}_0) . We consider next the time evolution of a second independent oscillator without feedback with an initial state $(t_0, \mathbf{m}_0 + \epsilon \hat{x})$, where the magnetization vector is slightly displaced toward the x axis by an infinitesimal ϵ . We then compute how the trajectories of these two oscillators (i.e., with and without feedback) diverge over a hundred periods. Regions where chaos is detected are denoted by ‘E’ in Fig. 3, where the dynamics comprises intermittent switching between the IPP and degenerate OPP states, with no well-defined periodicity. An example of the time dependence of the magnetization vector in this regime is shown in Fig. 4.

In order to gain a better understanding of this chaotic

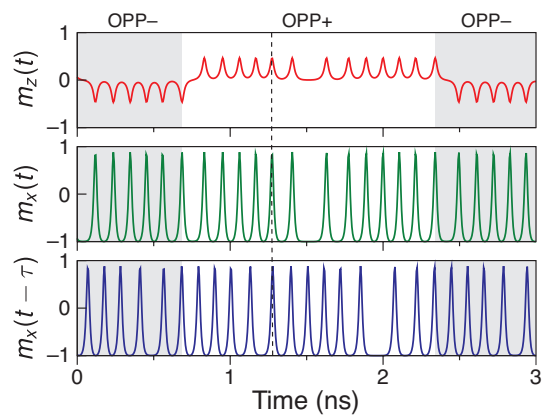


FIG. 5. Comparison of the time traces of the output and feedback signals in the chaotic regime (‘E’ in Fig. 3). There is a synchronization between output ($m_x(t)$) and feedback ($m_x(t - \tau)$) signals before every mode switching (straight line) but there are also some synchronization events not followed by a mode switching (dashed line).

regime, we examine the magnetization trajectories and feedback signals at the points where switching between the IPP and OPP modes take place. This is shown in Fig. 5, where $m_z(t)$, $m_x(t)$, and $m_x(t - \tau)$ are illustrated over several periods for $\tau = 0.5$ ns and $\Delta j = -100\%$. The main feature seen here is that mode switching almost always occurs after a temporary synchronization between the output and feedback signals, as indicated by the solid lines in the figure. The second highlighted synchronization (dashed line) on Figure 5 is not followed by a OPP+/OPP- or OPP/IPP switch, but we can see a slightly longer OPP+ period just after. This seems that the STNO is starting a mode switching from OPP+ to IPP or OPP- but is going back to OPP+, which is possible since the STNO has the same probability to go in either OPP+ or OPP- state. As such, it is possible to have OPP+/OPP+ and OPP-/OPP- transitions where a small transient phase occurs in between these states. This results in a jitter in the precession period, which may also impede subsequent synchronizations to the feedback signal.

Since non chaotic behavior implies a fixed phase difference between the output and feedback signals (in the form of the delay), and mode switching appears to be triggered by the synchronization of these two signals, it is interesting to examine how the phase difference between these two signals vary with the time delay. This is presented in Fig. 6, where the oscillator period, T , and phase difference with the feedback signal, is shown as a function of τ . T_0 denotes the precession period in the absence of chaos at $\Delta j = -0.1$. We note that other feedback strengths lead to the similar behavior and that certain aspects are analogous to the response to an ac current at fixed frequency.²⁹ The figure shows that the oscillator period exhibits large variations as a function of the delay, where the period almost doubles at small delays with deviations from the natural period decreasing with increasing delay. The appearance of the chaotic regime is intimately related to the phase difference between the feedback signal and the oscillator state. Consider first what happens when the regimes ‘A’ and ‘B’ are

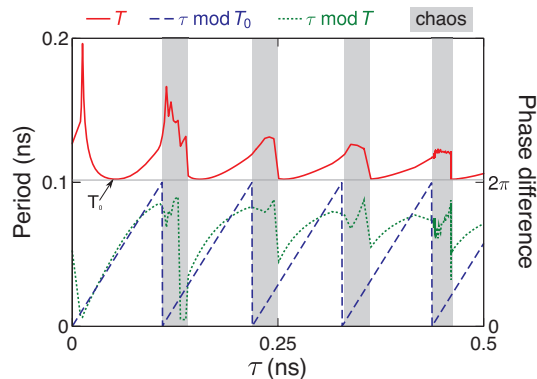


FIG. 6. Average precession period, T , and the phase difference between the oscillator output and feedback signal, as a function of the time delay τ . Chaos arises when the delay falls in a small interval exceeding the quantity $\tau \bmod T_0$, as indicated by the filled bands.

attained. Here, the phase difference between the oscillator and feedback signals remain constant at a value $\tau \bmod T$, where T is close to T_0 . Values of τ around a multiple of the natural period T_0 would therefore lead to a very small phase difference. However, we saw previously in Fig. 5 that temporary synchronization leads either to mode switching or a jitter in the period. For the former, the system does not attain a stable limit cycle, while for the latter the jitter results in increases in the average period until the stable limit cycle is reached. These two cases are illustrated in Fig. 6. For values of τ just below a multiple of T_0 (i.e., small negative phase differences), we observe increases in the average period leading to stable oscillations, while for small positive phase differences a chaotic regime is attained. This behavior is due to the fact that mode switching can only occur at certain points along the trajectory, much in the same way as periodic core reversal in nanocontact vortex oscillators,³⁰ so chaotic dynamics can only appear if the feedback signal produces such transitions at certain points along the trajectories.

With this in mind, let us now return to the discussion on regions ‘C’ and ‘D’. Here, the feedback delay is under a period and as such, there is always a small positive phase difference between the feedback and oscillator signals. The result is that the feedback triggers constant switching between the IPP and OPP states, but the overall behavior gives the impression of a stable IPP or OPP precession, as in regions ‘A’ and ‘B’.

Finally, regions ‘F’ and ‘G’ in Fig. 3 represent phenomena that only occur at long delays (more than 10 periods) and high feedback amplitudes. Such delays are comparable to the typical relaxation time toward the steady state orbit, i.e., the time required for initial transients associated with stable precession states like IPP or OPP to die out. ‘F’ represents a behavior in which transitions between the IPP and OPP states are seen. In contrast to ‘C’ and ‘D’, the oscillator remains in each of the IPP or OPP states for a longer duration, but switches intermittently between the two as in the chaotic state. An example of the time evolution is shown in Fig. 7. This figure depicts a typical time trace in the ‘F’ region where the feedback drives near-periodic switching between the IPP and OPP states. Af-

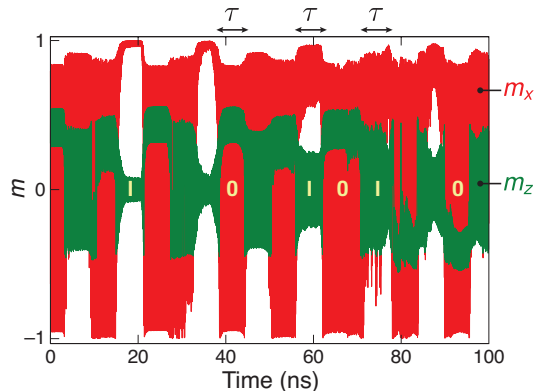


FIG. 7. Representative time trace of the unstable precession mode (‘F’ in Fig. 3). The oscillator switches between IPP (I) and OPP (O) modes with a period that is close to the delay τ .

ter each switching event, the oscillator relaxes toward a stable oscillatory state, but transients that reappear in the feedback signal after a long delay causes the system to switch to the other oscillation state. ‘G’ is similar, but describes transitions between the IPP state and the extinguished state, where no oscillations are present. This is similar to the ‘oscillator death’ scenario in systems of coupled limit-cycle oscillators.³¹ This behavior follows on from the different values of $\langle m_x \rangle$ attainable in the IPP phase (Fig 2), where $\langle m_x \rangle > 0$ combined with large $\Delta j < 0$ results in a suppression of the IPP mode and stabilization in the non-oscillatory state.

In summary, we have shown that delayed feedback in a macrospin spin-torque nano-oscillator can result in a variety of dynamical states, where transitions between different oscillation modes (such as in-plane and out-of-plane precession) can be triggered by using different delays and feedback amplitude. This is inherently possible due to the strongly nonlinear nature of magnetization dynamics, combined with the presence of multiple (and possibly degenerate) oscillatory states. The results suggest that delayed feedback may be a practical way for generating chaos and complex transient states in such oscillators, which might be useful for tasks such as fast random number generation^{32,33}, chaos multiplexing for cryptography,³⁴ and chaos-based computing.³⁵

ACKNOWLEDGMENTS

The authors acknowledge fruitful discussions with D. Rontani and M. Sciamanna. This work was partially supported by the Agence Nationale de la Recherche (France) under contract no. ANR-14-CE26-0021 (MEMOS). A.A. acknowledges support from Conselho Nacional de Desenvolvimento Científico e Tecnológico (CNPq, Brazil).

¹T. Chen, R. K. Dumas, A. Eklund, P. K. Muduli, A. Houshang, A. A. Awad, P. Dürrenfeld, B. G. Malm, A. Rusu, and J. Åkerman, *Proceedings of the IEEE* **104**, 1919 (2016).

²N. Locatelli, V. Cros, and J. Grollier, *Nature Materials* **13**, 11 (2013).

³F. Macià, A. D. Kent, and F. C. Hoppensteadt, *Nanotechnology* **22**, 095301 (2011).

- ⁴D. V. Berkov and J. Miltat, *Journal of Magnetism and Magnetic Materials* **320**, 1238 (2008).
- ⁵Z. Li and S. Zhang, *Physical Review B* **68**, 024404 (2003).
- ⁶J. Miltat, G. Albuquerque, and A. Thiaville, "An introduction to micro-magnetics in the dynamic regime," in *Spin Dynamics in Confined Magnetic Structures I*, edited by B. Hillebrands and K. Ounadjela (Springer, Berlin, Heidelberg, 2002) pp. 1–33.
- ⁷J.-V. Kim, in *Solid State Physics*, edited by R. E. Camley and R. L. Stamps (Academic Press, 2012) pp. 217–294.
- ⁸S. I. Kiselev, J. C. Sankey, I. N. Krivorotov, N. C. Emley, R. J. Schoelkopf, R. A. Buhrman, and D. C. Ralph, *Nature* **425**, 380 (2003).
- ⁹W. Rippard, M. Pufall, S. Kaka, S. Russek, and T. Silva, *Physical Review Letters* **92**, 027201 (2004).
- ¹⁰A. Slavin and V. Tiberkevich, *Physical Review Letters* **95**, 237201 (2005).
- ¹¹V. S. Pribiag, I. N. Krivorotov, G. D. Fuchs, P. M. Braganca, O. Ozatay, J. C. Sankey, D. C. Ralph, and R. A. Buhrman, *Nature Physics* **3**, 498 (2007).
- ¹²M. Pufall, W. Rippard, M. Schneider, and S. Russek, *Physical Review B* **75**, 140404 (2007).
- ¹³Q. Mistral, M. Van Kampen, G. Hrkac, J.-V. Kim, T. Devolder, P. Crozat, C. Chappert, L. Lagae, and T. Schrefl, *Physical Review Letters* **100**, 257201 (2008).
- ¹⁴A. Dussaux, B. Georges, J. Grollier, V. Cros, A. V. Khvalkovskiy, A. Fukushima, M. Konoto, H. Kubota, K. Yakushiji, S. Yuasa, K. A. Zvezdin, K. Ando, and A. Fert, *Nature Communications* **1**, 8 (2010).
- ¹⁵N. Locatelli, V. V. Naletov, J. Grollier, G. De Loubens, V. Cros, C. Deranlot, C. Ulysse, G. Faini, O. Klein, and A. Fert, *Applied Physics Letters* **98**, 062501 (2011).
- ¹⁶F. Garcia-Sanchez, J. Sampaio, N. Reyren, V. Cros, and J.-V. Kim, *New Journal of Physics* **18**, 075011 (2016).
- ¹⁷S. M. Mohseni, S. R. Sani, J. Persson, T. N. A. Nguyen, S. Chung, Y. Pogoryelov, P. K. Muduli, E. Iacocca, A. Eklund, R. K. Dumas, S. Bonetti, A. Deac, M. A. Hofer, and J. Åkerman, *Science* **339**, 1295 (2013).
- ¹⁸S. H. Strogatz, *Nonlinear Dynamics and Chaos* (Perseus Books, Reading, MA, 1994).
- ¹⁹M. C. Mackey and L. Glass, *Science* **197**, 287 (1977).
- ²⁰L. Appeltant, M. C. Soriano, G. Van der Sande, J. Danckaert, S. Massar, J. Dambre, B. Schrauwen, C. R. Mirasso, and I. Fischer, *Nature Communications* **2**, 468 (2011).
- ²¹Z. Li, Y. Li, and S. Zhang, *Physical Review B* **74**, 054417 (2006).
- ²²G. Khalsa, M. D. Stiles, and J. Grollier, *Applied Physics Letters* **106**, 242402 (2015).
- ²³S. Tamaru, H. Kubota, K. Yakushiji, A. Fukushima, and S. Yuasa, *Applied Physics Express* **9**, 053005 (2016).
- ²⁴S. Tsunegi, E. Grimaldi, R. Lebrun, H. Kubota, A. S. Jenkins, K. Yakushiji, A. Fukushima, P. Bortolotti, J. Grollier, S. Yuasa, and V. Cros, *Scientific Reports* **6**, 26849 (2016).
- ²⁵J. Xiao, A. Zangwill, and M. Stiles, *Physical Review B* **72**, 014446 (2005).
- ²⁶J. C. Slonczewski, *Journal of Magnetism and Magnetic Materials* **159**, L1 (1996).
- ²⁷J. Grollier, V. Cros, and A. Fert, *Physical Review B* **73**, 060409 (2006).
- ²⁸A. Wolf, J. B. Swift, H. L. Swinney, and J. A. Vastano, *Physica D: Nonlinear Phenomena* **16**, 285 (1985).
- ²⁹Y. Zhou, J. Persson, and J. Åkerman, *Journal of Applied Physics* **101**, 09A510 (2007).
- ³⁰S. Petit-Watelot, J.-V. Kim, A. Ruotolo, R. M. Otxoa, K. Bouzehouane, J. Grollier, A. Vansteenkiste, B. Van de Wiele, V. Cros, and T. Devolder, *Nature Physics* **8**, 682 (2012).
- ³¹P. Matthews and S. Strogatz, *Phys. Rev. Lett.* **65**, 1701 (1990).
- ³²W. Li, I. Reidler, Y. Aviad, Y. Huang, H. Song, Y. Zhang, M. Rosenbluh, and I. Kanter, *Physical Review Letters* **111**, 044102 (2013).
- ³³M. Virte, E. Mercier, H. Thienpont, K. Panajotov, and M. Sciamanna, *Optics Express* **22**, 17271 (2014).
- ³⁴E. Schöll and H. G. Schuster, *Handbook of Chaos Control* (Wiley-VCH, 1999).
- ³⁵W. L. Ditto, K. Murali, and S. Sinha, *Philosophical Transactions of the Royal Society A: Mathematical, Physical and Engineering Sciences* **366**, 653 (2008).